Taylor & Francis
Taylor & Francis Group

Particulate Science and Technology

An International Journal

ISSN: 0272-6351 (Print) 1548-0046 (Online) Journal homepage: www.tandfonline.com/journals/upst20

Optical, surface, and microstructural properties of $Li_4Ti_5O_{12}$ thin films coated by RF magnetron sputtering

H. Hakan Yudar, Suat Pat, Şadan Korkmaz, Soner Özen & Zerrin Pat

To cite this article: H. Hakan Yudar, Suat Pat, Şadan Korkmaz, Soner Özen & Zerrin Pat (2018) Optical, surface, and microstructural properties of $Li_4Ti_5O_{12}$ thin films coated by RF magnetron sputtering, Particulate Science and Technology, 36:8, 1037-1042, DOI: 10.1080/02726351.2017.1340378

To link to this article: https://doi.org/10.1080/02726351.2017.1340378

PARTICULATE SCIENCE AND TECHNOLOGY
2018, VOL. 36, NO. 8, 1037–1042
https://doi.org/10.1080/02726351.2017.1340378

Taylor & Francis
Taylor & Francis Group

Optical, surface, and microstructural properties of $Li_4Ti_5O_{12}$ thin films coated by RF magnetron sputtering

H. Hakan Yudar[a], Suat Pat[a], Şadan Korkmaz[a], Soner Özen[a], and Zerrin Pat[b]

[a]Physics Department, Eskişehir Osmangazi University, Eskişehir, Turkey; [b]Chemistry Department, Bilecik Seyh Edebali University, Bilecik, Turkey

ABSTRACT

$Li_4Ti_5O_{12}$ thin films were deposited on glass substrates by the RF magnetron sputtering method in an argon gas atmosphere at different powers. Some properties of the coated $Li_4Ti_5O_{12}$ films were examined using some techniques. Structural characteristics of the produced $Li_4Ti_5O_{12}$ films were investigated by X-ray diffraction. The $Li_4Ti_5O_{12}$ phases were identified as (311) and (222). The surface morphology of the produced $Li_4Ti_5O_{12}$ films was investigated using an atomic force microscope. The transmittance and the absorbance were measured using a UV–vis spectrophotometer. The transmittance values were around 88% and 90%. The absorbance values were approximately 0.053 and 0.048. The film thickness values were 140 and 50 nm. The transparency values of the produced films were high. The optical band gap values of the produced LTO films were calculated as ~3.8 eV. The refractive index and the reflectance spectra values of samples were determined using interferometer measurements. The refractive index values were 1.51 and 1.44 at 550 nm, respectively.

KEYWORDS

Anode materials; $Li_4Ti_5O_{12}$; plasma; RF magnetron sputter technique; thin film electrodes

Introduction

During the past century, energy has been produced by fossil fuels for the development of our industry, economy, and modern conveniences. Therefore, battery systems have been begun to develop for storing of extra produced energy. As a solution to this problem, the traditional lithium-ion battery system (LIBs) is developed. For the high security and energy storage, the developed battery is thought to have important long cycle life and good rate performance. The batteries have been applied in various portable equipment, electric and hybrid vehicles (Nitta et al. 2015). However, the traditional battery systems are not sufficient to meet the growing storage demands of the modern power system. In addition, the systems is unsafe and have short cycle life and low power density. Thus, recently, the search for battery systems has become important with high power density (Li et al. 2015), long cycle life (Li et al. 2015), and good safety (Jung et al. 2015) features. To solve such problems, it focuses on the development of solid state thin film battery systems. The electrode layer of the solid-state battery (SSB) is essential for the battery system. Lithium titanium oxide ($Li_4Ti_5O_{12}$) has recently attracted considerable attention as an anode material for SSB. $Li_4Ti_5O_{12}$ (LTO) has been regarded as an important alternative to anode materials for solid state batteries over recent years due to its long cycle life (Yao et al. 2011), thermal stability (Baba, Okada, and Yamaki 2002), excellent cycling performance (Tang et al. 2012), superior capacity retention (Choi and Manthiram 2006), and safety (Doughty and Roth 2012). At the same time, the LTO material is used for the production of electrochromic (EC) devices (Yu et al. 2010). Other EC materials used to produce devices are WO_3, NiO, TiO_2, and V_2O_5 (Wruck and Rubin 1993; Ahn et al. 2002; Sorar et al. 2013; Tong et al. 2015). The EC devices are called as smart technology. The devices are used for applications such as a smart window, rearview mirrors, imaging, and electronic paper (Svensson and Granqvist 1984; Chen, Lv, and Yi 2012; Buch, Chawla, and Rawal 2016). LTO thin films are prepared by a few techniques, for example, sol–gel (Kuo et al. 2016), chemical vapor deposition (Ling et al. 2014), RF magnetron sputtering (RF) (Wang et al. 2005), thermionic vacuum arc (TVA) (Pat et al. 2016), spray drying (Liu et al. 2015), hydrothermal (Hayashi, Nakamura, and Ebina 2014), molecular beam epitaxy (Lee et al. 2014), pulsed laser deposition (Oshima et al. 2015), vacuum evaporation (Muthukannan et al. 2016), electrodeposition (Wang et al. 2002), etc.

In this study, LTO thin films were produced at constant pressures, same times, and different powers. The optical and the surface properties of the produced films were observed. The suitable surface and crystallographic properties of the LTOs were examined for an anode layer of SSB. The optical properties of the LTOs were analyzed for a transparent anode layer of SSB. The sufficient thin layer was obtained for the SSB. These findings showed that the transparent anode layer of SSB can be used for RF technology, instead of complicated coating techniques.

Experimental

Prior to deposition, the surfaces of the glass substrate were cleaned in ethanol for 2 min and de-ionized water for 10 min and then the cleaned glasses were dried in air for 30 min. LTO was used as the material for this study. The used

CONTACT H. Hakan Yudar hakany@ogu.edu.tr Physics Department, Art and Science Faculty, Eskişehir Osmangazi University, 26480, Eskişehir, Turkey.
Color versions of one or more of the figures in the article can be found online at www.tandfonline.com/upst.

material had 99.9% purity, 50 diameters and 2 mm thickness such as a disk. The disk was put in the target of the sputter gun inside the vacuum chamber. Then, the dried glasses were placed in the sample holder as a substrate in a vacuum chamber. The distance between the target and the substrates was 25 mm in the chamber system. The chamber was evacuated to 10^{-3} Torr before the start of the RF magnetron sputter system. In the chamber, the LTO thin films were deposited using the RF magnetron sputter technique with argon gas (99.99%). The surfaces of all substrates were not heated during the production of the film. This experiment was conducted at the same pressure, different power, and about the same time. In the experiment, the pressure of vacuum chamber was set to 9×10^{-2} Torr for each sample. The overall deposition process was 65 min. Sample 1 (S1) and Sample 2 (S2) were produced at 75 and 85 W, respectively. Generally, deposited thin films by RF magnetron sputter have some properties such as homogeny, compact, high adherence, low crystalline dimension, uniform and nanostructure. The surface roughness of samples has been examined by an atomic force microscopy (Ambios Q-Scope). The AFM images of the film surface have been taken by non-contact mode using the Scan Atomic V 5.1.0 SPM control software. The absorbance and transmittance spectra of the LTO thin films were determined using UV–Vis spectrophotometers (UNICO 4802 double beam) in the spectral range of 200–1000 nm. The crystal structure of the coated samples was detected by X-ray diffraction (PANalytical Empyrean XRD) in the range of 10–70°. The Filmetrics F20 interferometer tool was used to measurement of the refractive index and the reflectance spectrum of coated LTO layers.

Results and discussion

The surface features of the LTO thin films were examined over $5 \times 5\ \mu m^2$ scanning areas with the AFM. In all measurements, scan angle and scan rates had 0° and 6 Hz at the AFM. The obtained AFM images of the surface of the film are shown in 2D and 3D for S1 and S2 in Figure 1.

As a result of this examination, the roughness parameters, which are the root mean square roughness (RMS), skewness (Ssk), and kurtosis (Skr) can be calculated for each two profile. The standard deviation of the surface of films from the average height is referred as RMS roughness. RMS value also can use for characterizing for optical of films surface. The RMS values indicate both the quality of the surface and the scattering of light. If the values of RMS are high, the surface roughness of films is loud. For mean RMS values roughness, different areas of each film need to measure room temperature. The RMS value of samples is measured as about 11.05 ± 4.66 and 8.40 ± 2.42 nm for S1 and S2, respectively. According to the result, S1 has a more surface roughness than S2. The Ssk and the Skr are the significant parameters for samples. While the Ssk is used to measure and understand the asymmetry of the height distribution of the films, the Skr means to measure and understand the smoothness of the films. The ideal Ssk value is zero. This value indicates a perfect symmetrical surface distribution. The Ssk may also have a positive value. This positive value implies many peaks and asymmetric of the height distribution. The Ssk may also have a negative value. This negative value means the existence of much planar valley and lot of small dip pits. As a result, the Ssk values of produced all samples were about 1.86 and 0.36 for $5 \times 5\ \mu m^2$ scanning areas, respectively. As a result of Skk values, for each sample, the surface has more peaks than flatness and the height of peaks is asymmetrical. While the Skr value is zero, the surface shows a normal dispersion. If the Skr is a positive value or negative value, surface morphology has a sharply peaked distribution or a flat-topped structure. For each of samples, The Skr values were obtained about 3.53–0.12 for $5 \times 5\ \mu m^2$ scanning areas, respectively. According to the Skr values, samples have sharp peaks on the topology of the surface. According to the RMS, the Skk and the Skr values, as the power increases, the surface becomes more homogeneous and uniform.

Figure 2 represents the optical properties and the crystal structures of the coated LTO. Figure 2 shows the absorption, the transmittance, the band gap and the XRD patterns of prepared thin films using RF sputtering technique. The transmittance and the absorption measurements were performed at room temperature. Figure 2a shows the absorbance values as 0.053 and 0.048 for S1 and S2. As can be seen in the Figure 2b, the transmittance values of S1 and S2 were observed 88 and 90% at 550 nm for S1 and S2, respectively. As this result, these samples have a transparent structure and indicate a good optical quality due to low absorption losses in the visible range. With the power increment, the transmittance increases at a small amount and the absorbance decreases. The transmittance values of the produced thin films are very high. The absorbance graph is low values. This result is in harmony with (Kim et al. 2013) and (Özen et al. 2016).

The absorption coefficients (α) were calculated using the measured transmittance (T) value. These coefficients are calculated by the following equation.

$$\alpha = (1/d)^{*}\log(1/T) \tag{1}$$

where d is the thickness of the coated LTO thin films (Pathak et al. 2016).

To identify the band gap energy of direct transition Tauc model was used. This method is expressed by the following equation.

$$\alpha h\upsilon = C(h\upsilon - E_g)^n \tag{2}$$

where α is the optical absorption coefficient, $h\upsilon$ (eV) is the incident photon energy, C is constant, $n = ½$ for direct transition and E_g (eV) is the optical band gap of the material (López et al. 2017).

Figure 2c shows the plot of $(\alpha h\upsilon)^2$ against $(h\upsilon)$ for LTO thin films. In the graph, the direct band gap values of the coated films appear to be almost equal. These values are 3.81 and 3.83 eV for each sample (Kim et al. 2013), respectively.

The PANalytical Empyrean XRD tool was used for crystallographic characterization of the coated LTO films at 75 and 85 W. The X-ray diffraction patterns of the produced LTO thin films at different RF powers can be seen in Figure 2d. The XRD patterns peak positions were found to be 41.84° and 44.40° for each sample. Corresponding miller indices for

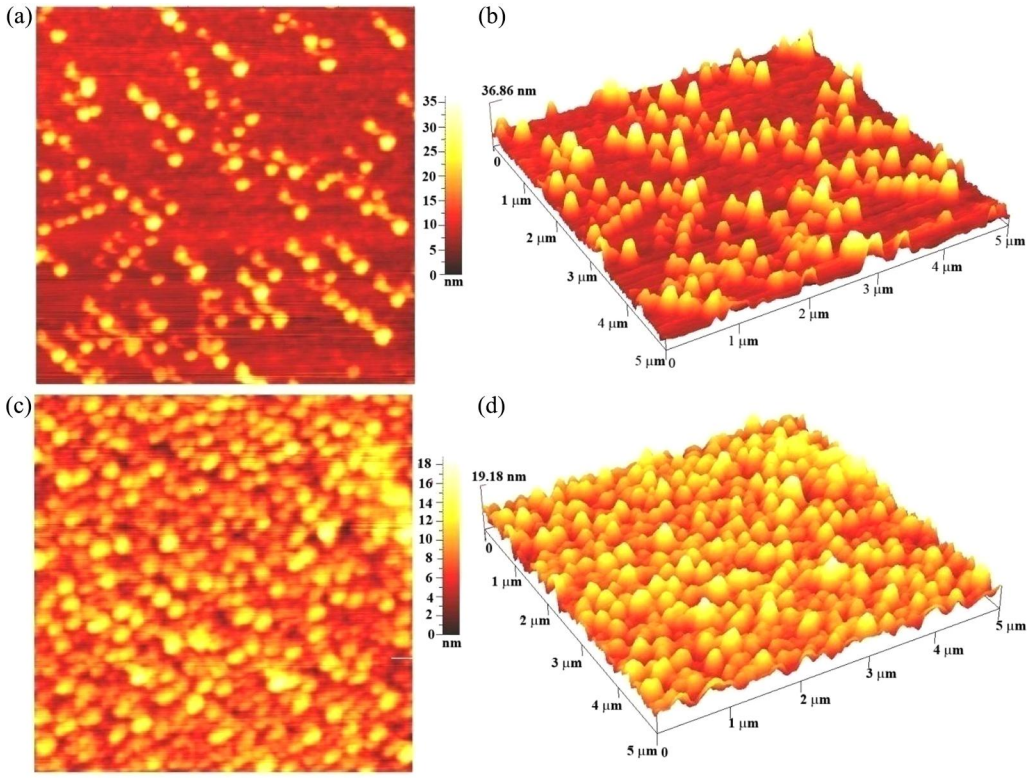

Figure 1. For S1 (a) 2D, (b) 3D of images of the LTO and for S2 (c) 2D, (d) 3D of images of LTO taken using AFM.

identified phases were found as (311) and (222) (Meng et al. 2013), respectively.

The Debye–Scherrer formula is used for calculating of the grain sizes. This formula is shown in the following equation:

$$D = K\lambda/\beta_{1/2}\cos\theta \tag{3}$$

where D is the crystallite diameter, K is a constant (0.94), λ is used X-ray wavelength (1.5406 Å), $\beta_{1/2}$ is the full width at half maximum (FWHM) of the observed peak (in radian), and θ is the diffraction angle of the selected peak (Kumar et al. 2016). The calculated as average crystallite sizes of the thin films were 26, 32, and 20 nm, 30 nm for S1 and S2, respectively.

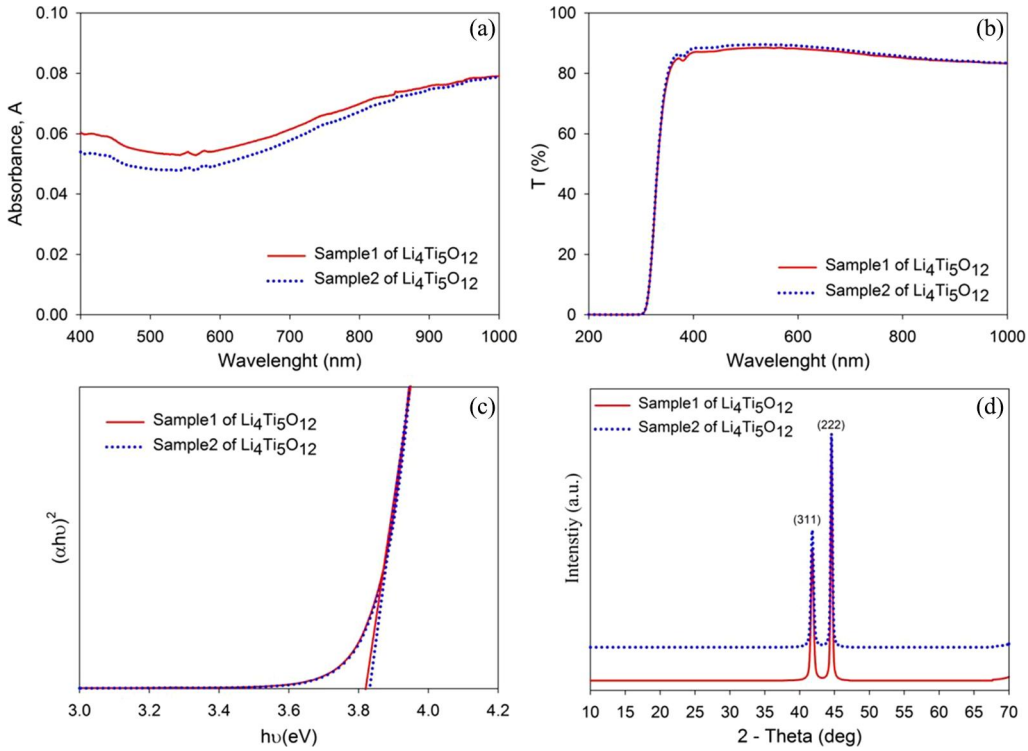

Figure 2. Absorbance (a), Transmittance spectra (b), Band gap (c) and XRD patterns (d) of the deposited LTO films.

Table 1. Some parameters of produced samples at different power.

Samples	Crystallite size (nm)	Lattice strain	Dislocation density (nm^{-2})	Thickness (nm)	Number of crystallites per unit volume (nm^{-2})
S1	26	0.0039	0.0015	140 ± 5	0.0079
	32	0.0030	0.0010	140 ± 5	0.0042
S2	20	0.0049	0.0025	50 ± 7	0.0062
	30	0.0033	0.0011	50 ± 7	0.0018

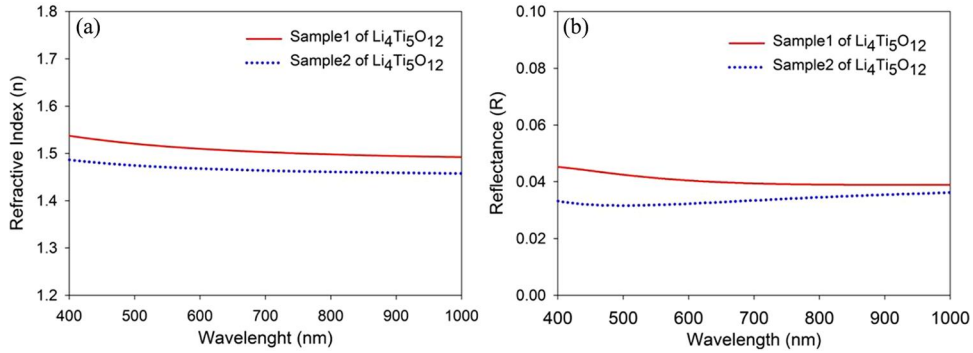

Figure 3. The refractive index (a) and the reflectance (b) spectra of coated LTO thin films on glass substrates.

The Relationship between dislocation density and calculated grain size values is given by in the following equation:

$$\delta = 1/D^2 \tag{4}$$

where δ is the dislocation density and D is the crystallite diameter (Korkmaz et al. 2016). For S1 and S2, dislocation density of the thin films was found as 0.0015, 0.0010, and 0.0025 nm^{-2}, 0.0011 nm^{-2}, respectively.

A number of crystallites per unit area for each prepared films was made with the following equation:

$$N = t/D^3\infty \tag{5}$$

where N is a number of crystallites per unit, t is the thickness of the films and D is crystallite diameter (Laatar et al. 2016). A number of crystallites per unit volume were approximately calculated 0.0079, 0.0042 and 0.0062, 0.0018 nm^{-2} for each two samples, respectively. All evaluated results are listed in Table 1. According to the results, the estimated crystallite size decreases when RF power increment. The crystal structures of the produced films are in harmony with the studies in the literature (Kim et al. 2013; Hayashi, Nakamura, and Ebina 2014; Liu et al. 2015; Kuo et al. 2016; Özen et al. 2016). Only lithium titanate and anatase TiO2 peaks are seen in the buildings. When we review the surface images, the thin films we produced are homogeneous and have low glare. And the crystal size ranges from 20 to 32 nm. This value is quite small compared to the grain sizes in (Kuo et al. 2016). The crystallite orientation and surface structure of the deposited layers directly play an important role the Li-ion diffusion capacity (Fujimoto et al. 2015; Kwon et al. 2017).

The refractive index and reflectance spectrum versus wavelength were given in Figure 3a and b show, respectively. One surface of the substrate was coated. Therefore, only the coated surface was measured. The refractive index values are in good agreement with films deposited by magnetron sputtering ($n \sim 1.5$ at 550 nm) (Özen et al. 2016). The refractive index values were about 1.51, 1.47 for the coated samples at 550 nm, respectively. In Figure 3a, when the wavelength values increase, the refractive index value decreases. This means that the measured data is well. In Figure 3b, the reflectance graph of coated films was plotted. It was seen that the mean reflection values of LTO coated the substrates were about 4 and 3% of each sample at 550 nm, respectively. As the power increased, the refractive values decreased.

The equation of the relation between the refractive index and the band gap is as follow:

$$n = \sqrt{\frac{12.417}{E_g - 0.365}} \tag{6}$$

where n is the refractive index and E_g is the band gap (Yudar et al. 2016). The calculated refractive index values are about 1.89.

Sum value of the optical reflection (R), the absorption (A) and the transmittance (T) is equal 7. This equation is given below:

$$R + T + A = 1 \tag{7}$$

The refractive index in order to obtained values is almost the same as the data. (Özen et al. 2016).

Zeiss supra 40 VP was used for the EDX analysis of the samples. Obtained results were summarized in Table 2. Li atoms cannot detect by this device. The higher amounts of the detected oxygen contents come from the substrate materials. Because, glass were used as substrate material.

Table 2. EDX analysis results.

Samples	Element	Series	Norm. C (wt %)	Atom. C (at. %)
S1	Oxygen	K-series	98.7	99.52
	Titanium	K-series	1.3	0.48
S2	Oxygen	K-series	98.75	96.4
	Titanium	K-series	1.25	3.6

Conclusions

LTO thin film was produced with successful by the RF magnetron sputtering technique in the duration of 65 min. This success makes it look as an alternative production method of the RF magnetron system for LTO thin films. The optical, the surface and the structural properties of the produced films were examined. According to the results, as the power increases, the film surface has more homogeneous, more uniform, more transmittance, less absorption, less reflection and smaller crystal sizes. Although the produced film has the characteristics in the literature, the refractive index and the reflectance of the films do not exist in the literature. In this paper, these deficiencies were tried to resolve. In order to obtained results and structural properties, these films are useful to utilize for solid state battery. The refractive index, the transmittance and the absorbance have suitable values for transparent solid state layer. The appropriate values for the transparent layer are high transmittance, low absorbance, low refractive index and thin thickness. Through an examination of the surface properties by AFM, the transparent surface of LTO can be selected for solid state battery. Suitable transparent LTO is the structure of having lowest roughness and most compact. In this respect, the produced LTO thin film can be used as an anode material for transparent solid-state lithium batteries.

Funding

This research activity was supported by TUBITAK (Grant number is 115E331).

References

Ahn, K.-S., Y.-C. Nah, Y.-E. Sung, K.-Y. Cho, S.-S. Shin, and J.-K. Park. 2002. All-solid-state electrochromic device composed of WO_3 and $Ni(OH)_2$ with a Ta_2O_5 protective layer. *Applied Physics Letters* 81 (21): 3930–32. doi:10.1063/1.1522478

Baba, Y., S. Okada, and J. Yamaki. 2002. Thermal stability of $LixCoO_2$ cathode for lithium ion battery. *Solid State Ionics* 148 (3):311–16. doi:10.1016/s0167-2738(02)00067-x

Buch, V. R., A. K. Chawla, and S. K. Rawal. 2016. Review on electrochromic property for WO_3 thin films using different deposition techniques. *Materials Today: Proceedings* 3 (6):1429–37. doi:10.1016/j.matpr.2016.04.025

Chen, X., Q. Lv, and X. Yi. 2012. Smart window coating based on nanostructured VO_2 thin film. *Optik-International Journal for Light and Electron Optics* 123 (13):1187–89. doi:10.1016/j.ijleo.2011.07.048

Choi, W., and A. Manthiram. 2006. Superior capacity retention spinel oxyfluoride cathodes for lithium-ion batteries. *Electrochemical and Solid-State Letters* 9 (5):A245–48. doi:10.1149/1.2186022

Doughty, D., and E. P. Roth. 2012. A general discussion of Li-ion battery safety. *Electrochemical Society Interface* 21 (2):37–44. doi:10.1149/2.f03122if

Fujimoto, D., N. Kuwata, Y. Matsuda, J. Kawamura, and F. Kang. 2015. Fabrication of solid-state thin-film batteries using $LiMnPO_4$ thin films deposited by pulsed laser deposition. *Thin Solid Films* 579:81–88. doi:10.1016/j.tsf.2015.02.041

Hayashi, H., T. Nakamura, and T. Ebina. 2014. Hydrothermal synthesis of $Li_4Ti_5O_{12}$ nanoparticles using a supercritical flow reaction system. *Journal of the Ceramic Society of Japan* 122 (1421):78–82. doi:10.2109/jcersj2.122.78

Jung, Y.-C., S.-K. Kim, M.-S. Kim, J.-H. Lee, M.-S. Han, D.-H. Kim, W.-C. Shin, M. Ue, and D.-W. Kim. 2015. Ceramic separators based on Li + -conducting inorganic electrolyte for high-performance lithium-ion batteries with enhanced safety. *Journal of Power Sources* 293:675–83. doi:10.1016/j.jpowsour.2015.06.001

Kim, C., N. S. Norberg, C. T. Alexander, R. Kostecki, and J. Cabana. 2013. Mechanism of phase propagation during lithiation in carbon-free $Li_4Ti_5O_{12}$ battery electrodes. *Advanced Functional Materials* 23 (9): 1214–22. doi:10.1002/adfm.201201684

Korkmaz, Ş., B. Geçici, S. D. Korkmaz, R. Mohammadigharehbagh, S. Pat, S. Özen, V. Şenay, and H. H. Yudar. 2016. Morphology, composition, structure and optical properties of CuO/Cu_2O thin films prepared by RF sputtering method. *Vacuum* 131:142–46. doi:10.1016/j.vacuum.2016.06.010

Kumar, V., M. Gohain, S. Som, V. Kumar, B. Bezuindenhoudt, and H. C. Swart. 2016. Microwave assisted synthesis of ZnO nanoparticles for lighting and dye removal application. *Physica B: Condensed Matter* 480:36–41. doi:10.1016/j.physb.2015.07.020

Kuo, Y.-C., H.-T. Peng, Y. Xiao, and J.-Y. Lin. 2016. Effect of starting materials on electrochemical performance of sol-gel-synthesized $Li_4Ti_5O_{12}$ anode materials for lithium-ion batteries. *Journal of Solid State Electrochemistry* 20:1625–31. doi:10.1007/s10008-016-3164-0

Kwon, N. H., H. Yin, T. Vavrova, J. H. Lim, U. Steiner, B. Grobéty, and K. M. Fromm. 2017. Nanoparticle shapes of $LiMnPO_4$, Li +diffusion orientation and diffusion coefficients for high volumetric energy Li +ion cathodes. *Journal of Power Sources* 342:231–40. doi:10.1016/j.jpowsour.2016.11.111

Laatar, F., A. Harizi, A. Smida, M. Hassen, and H. Ezzaouia. 2016. Effect of deposition temperature on the structural and optical properties of CdSe QDs thin films deposited by CBD method. *Materials Research Bulletin* 78:83–95. doi:10.1016/j.materresbull.2016.02.021

Lee, J., G. Luo, I. Tung, S. Chang, Z. Luo, M. Malshe, M. Gadre, A. Bhattacharya, S. Nakhmanson, and J. Eastman. 2014. Dynamic layer rearrangement during growth of layered oxide films by molecular beam epitaxy. *Nature materials* 13 (9):879–83. doi:10.1038/nmat4039

Li, R., Y. Wang, C. Zhou, C. Wang, X. Ba, Y. Li, X. Huang, and J. Liu. 2015. Carbon-stabilized high-capacity ferroferric oxide nanorod array for flexible solid-state alkaline battery–supercapacitor hybrid device with high environmental suitability. *Advanced Functional Materials* 25 (33):5384–94. doi:10.1002/adfm.201502265

Li, S., M. Ling, J. Qiu, J. Han, and S. Zhang. 2015. Anchoring ultra-fine TiO_2–SnO_2 solid solution particles onto graphene by one-pot ball-milling for long-life lithium-ion batteries. *Journal of Materials Chemistry A* 3 (18):9700–06. doi:10.1039/c5ta01350j

Ling, X., Y.-H. Lee, Y. Lin, W. Fang, L. Yu, M. S. Dresselhaus, and J. Kong. 2014. Role of the seeding promoter in MoS2 growth by chemical vapor deposition. *Nano Letters* 14 (2):464–72. doi:10.1021/nl4033704

Liu, W., Q. Wang, C. Cao, X. Han, J. Zhang, X. Xie, and B. Xia. 2015. Spray drying of spherical $Li_4Ti_5O_{12}$/C powders using polyvinyl pyrrolidone as binder and carbon source. *Journal of Alloys and Compounds* 621:162–69. doi:10.1016/j.jallcom.2014.09.121

López, J., E. Solorio, H. Borbón-Nuñez, F. Castillón, R. Machorro, N. Nedev, M. Farías, and H. Tiznado. 2017. Refractive index and bandgap variation in Al_2O_3-ZnO ultrathin multilayers prepared by atomic layer deposition. *Journal of Alloys and Compounds* 691:308–15. doi:10.1016/j.jallcom.2016.08.271

Meng, X., J. Liu, X. Li, M. N. Banis, J. Yang, R. Li, and X. Sun. 2013. Atomic layer deposited $Li_4Ti_5O_{12}$ on nitrogen-doped carbon nanotubes. *RSC Advances* 3 (20):7285–88. doi:10.1039/c3ra00033h

Muthukannan, A., P. Prema, J. Henry, K. Mohanraj, and G. Sivakumar. 2016. Photosensitivity of $CuBiSe_2$ thin film deposited by vacuum evaporation technique. *Journal of the Chinese Chemical Society* 63 (10):841–846.

Nitta, N., F. Wu, J. T. Lee, and G. Yushin. 2015. Li-ion battery materials: Present and future. *Materials Today* 18 (5):252–64.

Oshima, T., K. Yokoyama, M. Niwa, and A. Ohtomo. 2015. Pulsed-laser deposition of superconducting $LiTi_2O_4$ ultrathin films. *Journal of Crystal Growth* 419:153–57. doi:10.1016/j.jcrysgro.2015.03.029

Özen, S., V. Şenay, S. Pat, and Ş. Korkmaz. 2016. Optical, morphological properties and surface energy of the transparent $Li_4Ti_5O_{12}$ (LTO) thin

film as anode material for secondary type batteries. *Journal of Physics D: Applied Physics* 49 (10):105303. doi:10.1088/0022-3727/49/10/105303

Pat, S., Ş. Korkmaz, S. Özen, and V. Şenay. 2016. Heavily carbon doped GaAs nanocrystalline thin film deposited by thermionic vacuum arc method. *Journal of Alloys and Compounds* 657:711–16. doi:10.1016/j.jallcom.2015.10.150

Pathak, T. K., V. Kumar, L. Purohit, H. Swart, and R. Kroon. 2016. Substrate dependent structural, optical and electrical properties of ZnS thin films grown by RF sputtering. *Physica E: Low-dimensional Systems and Nanostructures* 84:530–36. doi:10.1016/j.physe.2016.06.020

Sorar, I., E. Pehlivan, G. A. Niklasson, and C. G. Granqvist. 2013. Electrochromism of DC magnetron sputtered TiO_2 thin films: Role of deposition parameters. *Solar Energy Materials and Solar Cells* 115:172–80. doi:10.1016/j.solmat.2013.03.035

Svensson, J., and C. Granqvist. 1984. Electrochromic coatings for smart windows. In 28th annual technical symposium, international society for optics and photonics. Optical Materials Technology for Energy Efficiency and Solar Energy Conversion III Carl M. Lampert, San Diego, August 21.

Tang, W., X. Gao, Y. Zhu, Y. Yue, Y. Shi, Y. Wu, and K. Zhu. 2012. A hybrid of V_2O_5 nanowires and MWCNTs coated with polypyrrole as an anode material for aqueous rechargeable lithium batteries with excellent cycling performance. *Journal of Materials Chemistry* 22 (38): 20143–45. doi:10.1039/c2jm34563c

Tong, Z., H. Lv, X. Zhang, H. Yang, Y. Tian, N. Li, J. Zhao, and Y. Li. 2015. Novel morphology changes from 3D ordered macroporous structure to V_2O_5 nanofiber grassland and its application in electrochromism. Scientific reports 5.

Wang, C., D. Wang, W. Chen, and Y. Wang. 2002. Tribological properties of nanostructured WC/CoNi and WC/CoNiP coatings produced by electro-deposition. *Wear* 253 (5):563–71. doi:10.1016/s0043-1648(02)00173-4

Wang, C.-L., Y. Liao, F. Hsu, N. Tai, and M. Wu. 2005. Preparation and characterization of thin film $Li_4Ti_5O_{12}$ electrodes by magnetron sputtering. *Journal of the Electrochemical Society* 152 (4):A653–57.

Wruck, D., and M. Rubin. 1993. Structure and electronic properties of electrochromic NiO films. *Journal of the Electrochemical Society* 140 (4):1097–104. doi:10.1149/1.2056205

Yao, Y., M. T. McDowell, I. Ryu, H. Wu, N. Liu, L. Hu, W. D. Nix, and Y. Cui. 2011. Interconnected silicon hollow nanospheres for lithium-ion battery anodes with long cycle life. *Nano Letters* 11 (7):2949–54. doi:10.1021/nl201470j

Yu, X., R. Wang, Y. He, Y. Hu, H. Li, and X. Huang. 2010. Electrochromic behavior of transparent $Li_4Ti_5O_{12}$/FTO electrode. *Electrochemical and Solid-State Letters* 13 (8):J99–101. doi:10.1149/1.3430658

Yudar, H. H., Ş. Korkmaz, S. Özen, V. Şenay, and S. Pat. 2016. Surface and optical properties of indium tin oxide layer deposition by RF magnetron sputtering in argon atmosphere. *Applied Physics A* 122 (8): 748. doi:10.1007/s00339-016-0262-x